Localization-delocalization transition in an electromagnetically induced photonic lattice

Rui Tian, Shuai Li, Maksims Arzamasovs,* Hong Gao, Yong-Chang Zhang, and Bo Liu†
Ministry of Education Key Laboratory for Nonequilibrium Synthesis and Modulation of Condensed Matter, Shaanxi Province Key Laboratory of Quantum Information and Quantum Optoelectronic Devices, School of Physics, Xi'an Jiaotong University, Xi'an 710049, China

(Received 8 May 2023; accepted 18 September 2023; published 16 October 2023)

We investigate the localization-delocalization transition (LDT) in an electromagnetically induced photonic lattice. A four-level tripod-type scheme in atomic ensembles is proposed to generate an effective photonic moiré lattice through the electromagnetically induced transparency (EIT) mechanism. By taking advantage of the tunable atomic coherence, we show that both periodic (commensurable) and aperiodic (incommensurable) structure can be created in such a photonic moiré lattice via adjusting the twist angle between two superimposed periodic patterns with square primitive. Furthermore, we also find that by tuning the amplitudes of these two superimposed periodic patterns, the localization-delocalization transition occurs for the light propagating in the aperiodic moiré lattice. Such localization is shown to link the fact that the flat bands of moiré lattice support quasi-nondiffracting localized modes and thus induce the localization of the initially localized beam. It would provide a promising approach to control the light propagation via the electromagnetically induced photonic lattice.

DOI: 10.1103/PhysRevA.108.043711

I. INTRODUCTION

Localized light waves can be used as a versatile tool for various types of manipulation and processing in optical information. It thus can be considered as a foundation for information dissemination. Past studies show that many promising methods, such as designing the optical localization propagation in optical fibers, utilizing artificial periodic structures in photonic crystals, and constructing random structures with Anderson localization effect, can implement light localization [1–5]. In particular, one of the key ingredients of these schemes is to engineer the spatial characteristics of the optical medium, which shows unprecedented capabilities in controlling the flow of light as well as matter waves [6–10].

Recently, another distinct approach to generating spatially periodic structures via the electromagnetically induced transparency (EIT) scheme [11], in either hot atomic vapors [12–14] or ultracold atoms [15], has attracted considerable attention. Various electromagnetically induced photonic lattices have been studied in previous works [13–21]. Many interesting physics, such as photonic Bloch oscillations [16], electromagnetically induced Talbot effect [17,18], topological defects in photonic graphene [19], optical edge-state solitons [20], and Klein paradox [21], have been explored.

In this work, we propose a four-level tripod-type scheme in atomic ensembles to generate an electromagnetically induced photonic moiré lattice [22,23] through the EIT mechanism. Since one can take advantage of the tunable atomic coherence in the EIT scheme, distinct from other schemes, such as utilizing the photorefractive crystal [22,23], it could provide new opportunities for exploring unveiled physics, such as the non-Hermition effect [24,25] and electromagnetically induced phase grating [26]. In the following, we will show that through changing the twist angle between two superimposed periodic patterns with square primitive in our proposed four-level tripod-type EIT scheme, the moiré pattern is highly flexible. Both periodic (commensurable) and aperiodic (incommensurable) structure can be achieved. Interestingly, we find a localization-delocalization transition (LDT) of the light propagating in the aperiodic photonic moiré lattice, which manifests the typical flat-band feature of the moiré lattice.

II. EFFECTIVE MODEL

Let us take the ^{87}Rb atomic system as an example to show our proposed four-level tripod-type scheme, which is schematically presented in Fig. 1(a). The signal, coupling, and pump fields drive the transitions $|1\rangle \rightarrow |4\rangle$, $|2\rangle \rightarrow |4\rangle$, and $|3\rangle \rightarrow |4\rangle$, respectively, where $|1\rangle$, $|2\rangle$, and $|3\rangle$ can be chosen from the $5^2S_{1/2}$ state of ^{87}Rb, such as $|F = 1, m_F = \pm 1\rangle$ and $|F = 2, m_F = 1\rangle$, while $|4\rangle$ can be selected from the $5^2P_{1/2}$ state, such as $|F' = 1, m_F = 0\rangle$. Here we consider that both the signal and pump beams are injected into atomic ensemble along the z axis. The coupling field is consisted of two groups of orthogonalized paired beams paraxially propagating along the z direction.

Under the rotating-wave approximation, the density-matrix equations for our proposed four-level tripod-type atomic system can be expressed as [27]

$$\dot{\rho}_{11} = -\frac{i}{2}\Omega_s\rho_{14} + \frac{i}{2}\Omega_s^*\rho_{41} + \Gamma_{41}\rho_{44}$$

$$\dot{\rho}_{22} = -\frac{i}{2}\Omega_c\rho_{24} + \frac{i}{2}\Omega_c^*\rho_{42} + \Gamma_{42}\rho_{44}$$

*max.arzamasov@me.com
†liubophy@gmail.com

$$
\begin{aligned}
\dot{\rho}_{33} =& -\frac{i}{2}\Omega_p\rho_{34} + \frac{i}{2}\Omega_p^*\rho_{34}\rho_{43} + \Gamma_{43}\rho_{44} \\
\dot{\rho}_{44} =& \frac{i}{2}(\Omega_s\rho_{14} - \Omega_s^*\rho_{41}) + \frac{i}{2}(\Omega_c\rho_{24} - \Omega_c^*\rho_{42}) \\
&+ \frac{i}{2}(\Omega_p\rho_{34} - \Omega_p^*\rho_{43}) - \Gamma\rho_{44} \\
\dot{\rho}_{21} =& i(\Delta_s - \Delta_c)\rho_{21} + \frac{i}{2}\Omega_c^*\rho_{41} - \frac{i}{2}\Omega_s\rho_{24} \\
\dot{\rho}_{31} =& i(\Delta_s - \Delta_p)\rho_{31} + \frac{i}{2}\Omega_p^*\rho_{41} - \frac{i}{2}\Omega_s\rho_{34} \\
\dot{\rho}_{41} =& \frac{i}{2}\Omega_s\rho_{11} + \frac{i}{2}\Omega_c\rho_{21} + \frac{i}{2}\Omega_p\rho_{31} - \frac{i}{2}\Omega_s\rho_{44} \\
&+ i\Delta_s\rho_{41} - \frac{\Gamma}{2}\rho_{41} \\
\dot{\rho}_{32} =& i(\Delta_c - \Delta_p)\rho_{32} + \frac{i}{2}\Omega_p^*\rho_{42} - \frac{i}{2}\Omega_c\rho_{34} \\
\dot{\rho}_{42} =& \frac{i}{2}\Omega_s\rho_{12} + \frac{i}{2}\Omega_c\rho_{22} + \frac{i}{2}\Omega_p\rho_{32} - \frac{i}{2}\Omega_c\rho_{44} \\
&+ i\Delta_c\rho_{42} - \frac{\Gamma}{2}\rho_{42} \\
\dot{\rho}_{43} =& \frac{i}{2}\Omega_s\rho_{13} + \frac{i}{2}\Omega_c\rho_{23} + \frac{i}{2}\Omega_p\rho_{33} - \frac{i}{2}\Omega_p\rho_{44} \\
&+ i\Delta_p\rho_{43} - \frac{\Gamma}{2}\rho_{43}, \qquad (1)
\end{aligned}
$$

where Γ_{nm} is the natural decay rate between levels $|n\rangle$ and $|m\rangle$ and $\Gamma = \Gamma_{41} + \Gamma_{42} + \Gamma_{43}$. $\Omega_s = \mu_{41}E_s/\hbar$, $\Omega_c = \mu_{42}E_c/\hbar$, and $\Omega_p = \mu_{43}E_p/\hbar$ are Rabi frequencies of the signal, coupling, and pump fields, where μ_{ij} is the electric dipole matrix element related to the atomic transition between $|i\rangle$ and $|j\rangle$. $E_{s(c,p)}$ is the strength of the corresponding electric field. $\Delta_s = \omega_s - \omega_{14}$, $\Delta_c = \omega_c - \omega_{24}$, and $\Delta_p = \omega_p - \omega_{34}$ denote the frequency detunings. Since the signal field is much weaker than both the coupling and pump fields, from Eq. (1) we can obtain the following relations:

$$
\begin{aligned}
\rho_{21} &= \frac{-\Omega_c^*/2}{\Delta_s - \Delta_c}\rho_{41} \\
\rho_{31} &= \frac{-\Omega_p^*/2}{\Delta_s - \Delta_p}\rho_{41}. \qquad (2)
\end{aligned}
$$

Substituting Eq. (2) into Eq. (1), ρ_{41} can be solved as

$$
\rho_{41} = -\left[\left(\Delta_s + \frac{i\Gamma}{2}\right) + \frac{|\Omega_c|^2/4}{\Delta_c - \Delta_s} + \frac{|\Omega_p|^2/4}{\Delta_p - \Delta_s}\right]^{-1}\frac{\Omega_s}{2}. \qquad (3)
$$

The susceptibility of atomic medium can be determined through the following formula:

$$
\begin{aligned}
\chi &= 2N\mu_{14}\rho_{41}/\epsilon_0 E_s \\
&= \frac{-N|\mu_{14}|^2}{\epsilon_0}\left[\left(\Delta_s + \frac{i\Gamma}{2}\right) + \frac{|\Omega_c|^2/4}{\Delta_c - \Delta_s} + \frac{|\Omega_p|^2/4}{\Delta_p - \Delta_s}\right]^{-1}, \qquad (4)
\end{aligned}
$$

where N is the atomic density. In this work, we consider the case with $\Delta_s \neq \Delta_{c,p}$ to avoid the transparency window

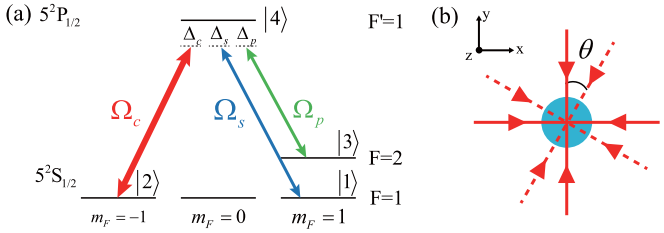

FIG. 1. (a) The schematic plot of our proposed four-level tripod scheme. Here $\Omega_{s(p,c)}$ stands for the Rabi frequencies of the signal, pump, and coupling fields, respectively. $\Delta_{s(p,c)}$ labels the corresponding frequency detuning. (b) Two groups of orthogonalized paired-standing waves marked by the solid and dashed lines, respectively, which can form two superimposed square patterns. θ labels the twisted angle between them.

in the EIT scheme. The refractive index can be obtained via the relation $n = \sqrt{1+\chi} \approx 1 + \chi/2$. From Eq. (4), one can notice that the spatial profile of the susceptibility is highly dependent on the distribution of the coupling fields, and thus can produce various structures by shaping them. To show that, here we consider that the coupling fields are consisted of two groups of orthogonalized paired standing waves paraxially propagating along the z axis (captured by a small angle ϕ to the z axis), as depicted in Fig. 1(b) by the solid and dashed lines, respectively. Distinct from the previous studies [13–21], the key idea here is to design the spatial structure of the coupling fields. Two groups of orthogonalized paired standing waves can form two superimposed square patterns. And the total spatial pattern is highly tunable through changing the twisted angle as shown in Fig. 1(b). To be more specific, the four standing waves as shown in Fig. 1(b) can be expressed as

$$
\begin{aligned}
\vec{E}_{c1}(\vec{r},t) &= E_c' \cos k_0 x\left[e^{i(k_z z - \omega_c t)}\hat{x} + e^{i(k_z z - \omega_c t - \pi/2)}\hat{y}\right] \\
\vec{E}_{c2}(\vec{r},t) &= E_c' \cos k_0 y\left[e^{i(k_z z - \omega_c t + \pi/2)}\hat{x} + e^{i(k_z z - \omega_c t)}\hat{y}\right] \\
\vec{E}_{c3}(\vec{r},t) &= E_c'' \cos k_0 x'\left[e^{i(k_z z - \omega_c t)}\hat{x}' + e^{i(k_z z - \omega_c t - \pi/2)}\hat{y}'\right] \\
\vec{E}_{c4}(\vec{r},t) &= E_c'' \cos k_0 y'\left[e^{i(k_z z - \omega_c t + \pi/2)}\hat{x}' + e^{i(k_z z - \omega_c t)}\hat{y}'\right], \qquad (5)
\end{aligned}
$$

where $k_z = k_c \cos\phi$ and $k_0 = k_c \sin\phi$. Unit vectors $\hat{x}', \hat{y}'$ are related to $\hat{x}, \hat{y}$ via the relation $[x', y']^{\mathsf{T}} = S[x, y]^{\mathsf{T}}$, where $S = [\cos\theta, -\sin\theta; \sin\theta, \cos\theta]$ is the operator of two-dimensional (2D) rotation. Therefore, the intensity of the coupling field can be expressed as

$$
\begin{aligned}
|E_c(x,y)|^2 =& 2E_c'^2|[\cos(k_0 y)\hat{x} + \cos(k_0 x)\hat{y}] \\
&+ \alpha[\cos(k_0 y')\hat{x}' + \cos(k_0 x')\hat{y}']|^2, \qquad (6)
\end{aligned}
$$

where $\alpha = E_c''/E_c'$. As shown in Fig. 2, when varying the twisted angle θ and amplitude ratio α, the interference of coupling fields will produce different spatial patterns and induce an effective 2D photonic lattice in the xy plane. For instance, the periodic structure of refractive index lattice is produced when θ is a Pythagorean angle, e.g., $\theta = \arctan 4/3$ [see Figs. 2(b) and 2(d); otherwise, the aperiodic structure is induced, e.g., $\theta = \pi/6$ [see Figs. 2(a) and 2(c)].

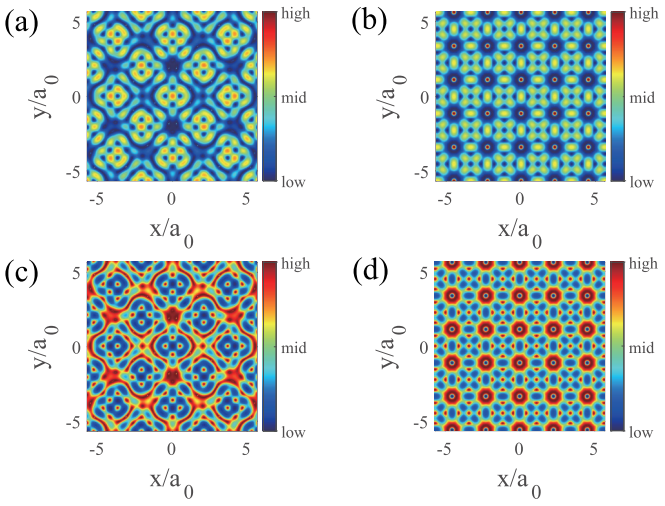

FIG. 2. Spatial structure of the refractive index lattice. (a) and (c) show the real and imaginary part of the refractive index lattice with $\theta = \pi/6$, which forms an aperiodic moiré pattern. For comparison, a periodic structure is also shown in (b) and (d) for the real part and imaginary part with $\theta = \arctan 4/3$. Here $a_0 = \lambda_c/\sin\phi$ and $\alpha = 1$. The detunings are chosen as $\Delta_s \neq \Delta_{c,p}$ to avoid the transparency window in the EIT scheme.

III. LOCALIZATION-DELOCALIZATION TRANSITION

In the following, we will demonstrate the effect of the spatial profiles of our proposed refractive index lattice through investigating the light propagation within it. The propagation of signal beam $\vec{E}_s(\vec{r},t)$ in the atomic medium is governed by the following electric field wave equation:

$$\nabla^2\vec{E}_s + \frac{\omega_s^2}{c^2}\epsilon(\vec{r})\vec{E}_s = 0, \tag{7}$$

where $\epsilon = 1+\chi$ is the relative dielectric constant. We then rewrite $\vec{E}_s(\vec{r},t)$ as $\vec{E}_s(\vec{r},t) = \psi(\vec{r})[\exp(ik_sz - i\omega_st)\hat{x} + \exp(ik_sz - i\omega_st + \pi/2)\hat{y}]$, with $\psi(\vec{r})$ being the field amplitude. Then, from Eq. (7) a Schrödinger-type equation of $\psi(\vec{r})$ can be obtained,

$$i\frac{\partial}{\partial z}\psi = -\frac{1}{2k_s}\left(\frac{\partial^2}{\partial x^2} + \frac{\partial^2}{\partial y^2}\right)\psi - \frac{k_s\Delta n(x,y)}{n_0}\psi, \tag{8}$$

where $\Delta n(x,y) \approx \chi/2$ and $k_s = 2\pi n_0/\lambda_s$ is the wave vector of the signal beam. n_0 is the ambient refractive index.

To investigate the light propagation in the refractive index lattices as shown in Fig. 2, we initialize the signal beam as a Gaussian wave packet and numerically simulate its propagation. As shown in Fig. 3, when θ is chosen as a Pythagorean angle—for instance, $\theta = \arctan 4/3$—the refractive index lattices possess a spatially periodic structure and the initial Gaussian wave packet displays the delocalization behavior

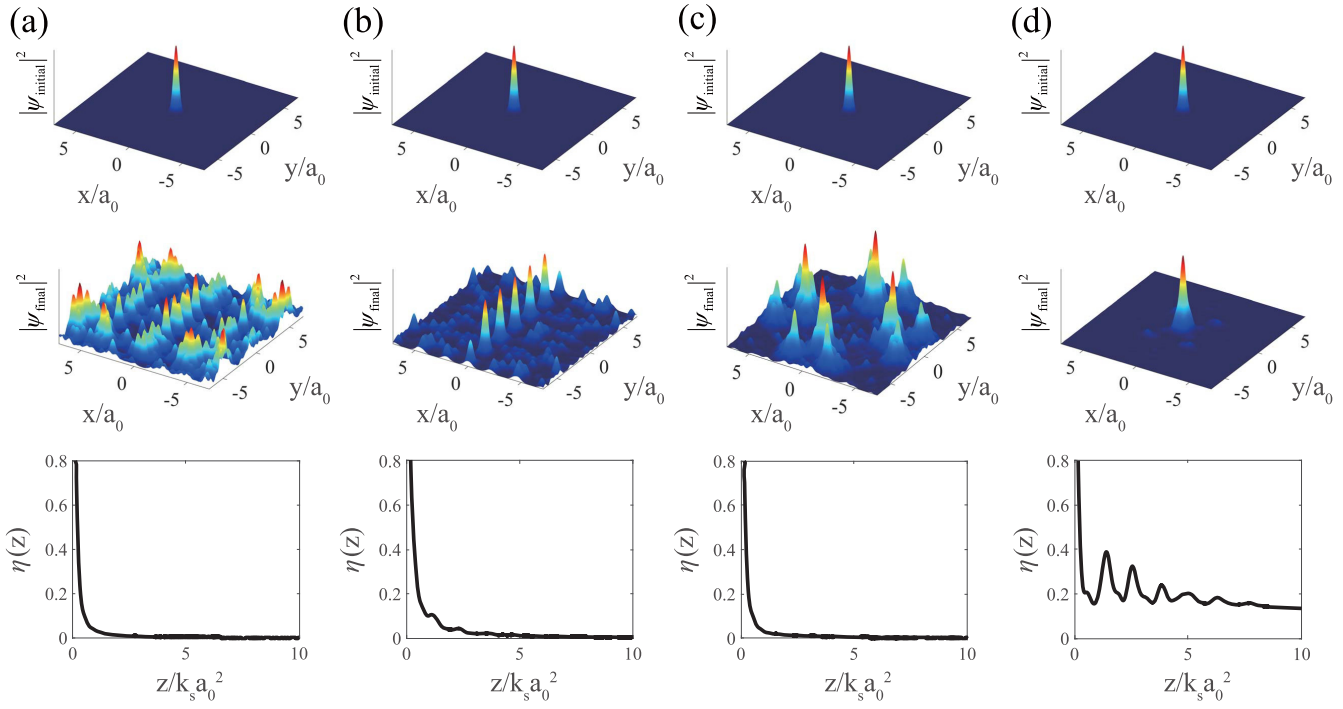

FIG. 3. The propagation of light in moiré photonic lattice. In (a) and (b), it is shown that when θ is chosen as a Pythagorean angle $\theta = \arctan 4/3$, the initial Gaussian wave packet (top row) displays the delocalized behavior for any amplitude ratio α of two superimposed periodic patterns. Here, we choose $\alpha = 0.1$ and $\alpha = 1$ in (a) and (b), respectively. Such delocalized behavior can also be captured by the vanished IPR with the long propagation distance, as shown in the bottom row of (a) and (b). In (c) and (d), when $\theta = \pi/6$, we find that there is a threshold of α. Below that threshold, as shown in the middle panel of (c) ($\alpha = 0.1$), the light propagation still shows the delocalized behavior, while above that threshold, as shown in the middle row of (d) ($\alpha = 1$), the light propagation will still keep being localized, which can be verified by the nonzero IPR as shown in the bottom row of (d). In the middle row, the propagation distance is chosen as $z/k_sa_0^2 = 10$. Other parameters are chosen as the same as in Fig. 2.

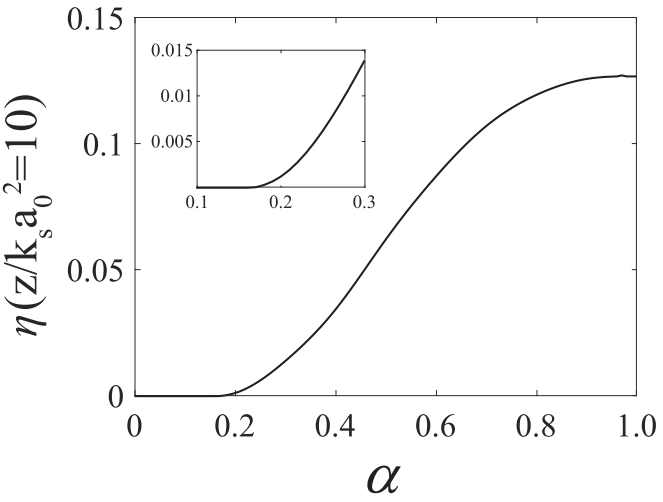

FIG. 4. IPR as a function of the amplitude ratio α of two superposed patterns for aperiodic moiré lattice. A threshold of amplitude ratio α can be determined by the nonzero point of IPR. Other parameters are chosen as the same as in Fig. 3(d)

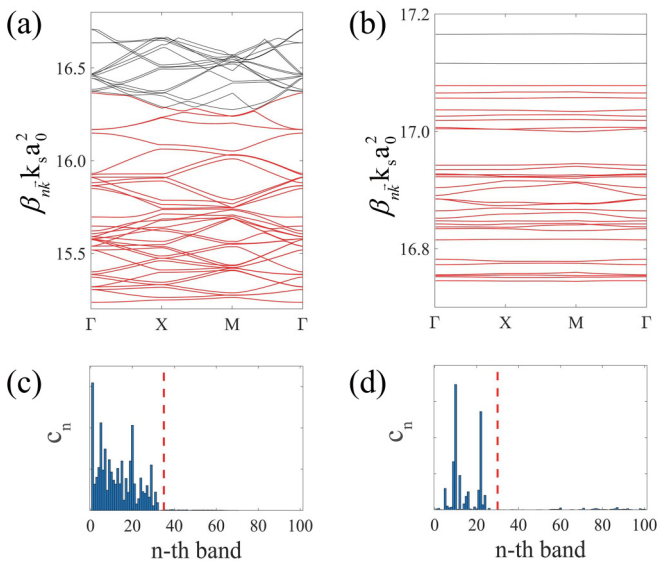

FIG. 5. [(a), (b)] The single-particle dispersion relation of aperiodic lattice with $\theta = \pi/6$ under the Pythagorean approximation via choosing $\theta = \arctan 120/209$ for $\alpha = 0.1$ and $\alpha = 1.0$, respectively. [(c), (d)] The band occupation probability c_n defined in the main text for the case with $\alpha = 0.1$ and $\alpha = 1.0$, respectively. In (a) and (b), the red bands are the occupied bands of the chosen initial wave packet.

for arbitrary amplitude ratio α of the two superimposed periodic patterns. When the refractive index lattices possess a spatial aperiodic structure—for instance, $\theta = \pi/6$—we find that there is a threshold of α. Below that threshold, as shown in Fig. 3(c), the light propagation still shows the delocalization behavior. However, if α exceeds the threshold, as shown in Fig. 3(d), the signal beam turns out to be localized. Therefore, there is a LDT in aperiodic moiré lattice when tuning the amplitudes of the two superimposed periodic patterns. To quantitatively analyze the LDT here, we introduce the factor inverse participation ratio (IPR) [28] defined as $\eta(z) = \int |\psi(\vec{r})|^4 dxdy / [\int |\psi(\vec{r})|^2 dxdy]^2$. The localized behavior can be captured by the nonzero IPR. As shown in Fig. 4, the threshold of amplitude ratio in the aperiodic moiré lattice separating two distinct regimes in the LDT can be determined by the nonzero point of IPR when varying α. Actually, the transition point of α is dependent on the initial state, which is distinct from the analysis of the localized properties of the equilibrium eigenmodes in the previous studies [22,23].

To understand the localization of light in aperiodic moiré lattice, we calculate its single-particle dispersion relation through approximating the non-Pythagorean twist angle by a Pythagorean one [22]. For instance, here we use $\theta = \arctan(120/209)$ to approximate $\theta = \pi/6$. Under such an approximation, the single-particle dispersion of aperiodic lattice can be obtained by the plane-wave expansion method through introducing the Bloch basis $\psi_{n\vec{k}} = \sum_{\vec{G}} u_{n\vec{k},\vec{G}} |\vec{k} + \vec{G}\rangle$ with the Bloch vector $\vec{k}$ and reciprocal lattice vector $\vec{G}$. Here n labels the band index. Then, the single-particle dispersion relation can be obtained through solving the eigenproblem via the following relation:

$$\frac{(\vec{k}+\vec{G})^2}{2k_s} u_{n\vec{k},\vec{G}} - \frac{k_s}{n_0} \sum_{\vec{G}'} \langle \vec{k}+\vec{G}|\Delta n(x,y)|\vec{k}+\vec{G}'\rangle u_{n\vec{k},\vec{G}'} = \beta_{n\vec{k}} u_{n\vec{k},\vec{G}}, \tag{9}$$

where $\beta_{n\vec{k}}$ is the dispersion relation of 2D Bloch waves. As shown in Fig. 5, when the amplitude ratio α increases, more lower bands become extremely flat. Since the flat bands support quasi-nondiffracting localized modes, the initially localized beam launched into such moiré lattice will remain localized. To show that, we define a quantity $c_n \equiv \langle \psi_n | \psi_0 \rangle$, with $|\psi_0\rangle$ labeling the initial Gaussian wave packet and $|\psi_n\rangle$ standing for the eigenstates solved from Eq. (9), to decompose the initial state into the eigenstates of aperiodic lattice. It can capture the band occupation probability of the chosen initial state. For instance, as shown in Figs. 5(a) and 5(c), when the amplitude ratio α is below the threshold, the occupied bands of the initial wave packet ($c_n \neq 0$) are dispersive. Therefore, the light propagator presents the delocalized behavior. While increasing α above the threshold, the occupied bands of the initial wave packet are flat. Therefore, such flat bands drive the LDT in aperiodic moiré lattice, since the flat bands support quasi-nondiffracting localized modes.

IV. CONCLUSION

In summary, we propose a four-level tripod-type EIT scheme in atomic ensembles to induce a photonic moiré lattice. Such a lattice shows great tunability of changing the spatial structure. Both periodic and aperiodic structures can be achieved. We further explore the LDT behavior in the aperiodic moiré lattice through investigating the light propagation. A threshold of amplitude ratio of two superposed patterns has been found. Such a phenomenon can be understood through analysis of the flat-band physics of moiré lattice. Our proposal would provide a promising approach to manipulate the light propagation through electromagnetically induced

photonic lattices and thus have potential applications in optical information techniques.

ACKNOWLEDGMENTS

This work is supported by the National Key R&D Program of China (Grant No. 2021YFA1401700), the NSFC (Grants No. 12074305, No. 12147137, and No. 11774282), the Xiaomi Young Scholar Program (R.T., S.L., M.A., and B.L.), and Shaanxi Academy of Fundamental Sciences (Mathematics, Physics) (Grant No. 22JSY036), Xi'an Jiaotong University, through the Young Top Talents Support Plan, Basic Research Funding (Grant No. xtr042021012) (Z.C.). We also thank the HPC platform of Xi'An Jiaotong University, where our numerical calculations were performed.

[1] T. Schwartz, G. Bartal, S. Fishman, and M. Segev, Nature (London) **446**, 52 (2007).
[2] Y. Lahini, A. Avidan, F. Pozzi, M. Sorel, R. Morandotti, D. N. Christodoulides, and Y. Silberberg, Phys. Rev. Lett. **100**, 013906 (2008).
[3] Y. Lahini, R. Pugatch, F. Pozzi, M. Sorel, R. Morandotti, N. Davidson, and Y. Silberberg, Phys. Rev. Lett. **103**, 013901 (2009).
[4] A. Szameit, Y. Kartashov, P. Zeil, F. Dreisow, M. Heinrich, R. Keil, S. Nolte, A. Tünnermann, V. Vysloukh, and L. Torner, Opt. Lett. **35**, 1172 (2010).
[5] L. Levi, M. Rechtsman, B. Freedman, T. Schwartz, O. Manela, and M. Segev, Science **332**, 1541 (2011).
[6] Y. S. Kivshar and G. P. Agrawal, *Optical Solitons: From Fibers to Photonic Crystals* (Academic Press, New York, 2003).
[7] R. D. V. Meade, S. G. Johnson, and J. N. Winn, *Photonic Crystals: Molding the Flow of Light* (Princeton University Press, Princeton, 2008).
[8] I. L. Garanovich, S. Longhi, A. A. Sukhorukov, and Y. S. Kivshar, Phys. Rep. **518**, 1 (2012).
[9] C. W. Hsu, B. Zhen, J. Lee, S.-L. Chua, S. G. Johnson, J. D. Joannopoulos, and M. Soljačić, Nature (London) **499**, 188 (2013).
[10] Y. V. Kartashov, G. E. Astrakharchik, B. A. Malomed, and L. Torner, Nat. Rev. Phys. **1**, 185 (2019).
[11] H. Y. Ling, Y.-Q. Li, and M. Xiao, Phys. Lett. A **57**, 1338 (1998).
[12] A. W. Brown and M. Xiao, Opt. Lett. **30**, 699 (2005).
[13] J. Sheng, J. Wang, M.-A. Miri, D. N. Christodoulides, and M. Xiao, Opt. Express **23**, 19777 (2015).
[14] Z. Zhang, J. Feng, X. Liu, J. Sheng, Y. Zhang, Y. Zhang, and M. Xiao, Opt. Lett. **43**, 919 (2018).
[15] H. Zhang, J. Yuan, S. Dong, C. Wu, and L. Wang, Appl. Sci. **10**, 5740 (2020).
[16] Y. Zhang, D. Zhang, Z. Zhang, C. Li, Y. Zhang, F. Li, M. R. Belić, and M. Xiao, Optica **4**, 571 (2017).
[17] Z. Zhang, X. Liu, D. Zhang, J. Sheng, Y. Zhang, Y. Zhang, and M. Xiao, Phys. Rev. A **97**, 013603 (2018).
[18] S. Ning, J. Lu, S. Liang, Y. Feng, C. Li, Z. Zhang, and Y. Zhang, Opt. Lett. **46**, 5035 (2021).
[19] Z. Zhang, F. Li, G. Malpuech, Y. Zhang, O. Bleu, S. Koniakhin, C. Li, Y. Zhang, M. Xiao, and D. D. Solnyshkov, Phys. Rev. Lett. **122**, 233905 (2019).
[20] Z. Zhang, R. Wang, Y. Zhang, Y. V. Kartashov, F. Li, H. Zhong, H. Guan, K. Gao, F. Li, Y. Zhang *et al.*, Nat. Commun. **11**, 1902 (2020).
[21] Z. Zhang, Y. Feng, F. Li, S. Koniakhin, C. Li, F. Liu, Y. Zhang, M. Xiao, G. Malpuech, and D. Solnyshkov, Phys. Rev. Lett. **129**, 233901 (2022).
[22] P. Wang, Y. Zheng, X. Chen, C. Huang, Y. V. Kartashov, L. Torner, V. V. Konotop, and F. Ye, Nature (London) **577**, 42 (2020).
[23] Q. Fu, P. Wang, C. Huang, Y. V. Kartashov, L. Torner, V. V. Konotop, and F. Ye, Nat. Photon. **14**, 663 (2020).
[24] J. Sheng, M.-A. Miri, D. N. Christodoulides, and M. Xiao, Phys. Rev. A **88**, 041803(R) (2013).
[25] Z. Zhang, L. Yang, J. Feng, J. Sheng, Y. Zhang, Y. Zhang, and M. Xiao, Laser Photonics Rev. **12**, 1800155 (2018).
[26] S. H. Asadpour, H. R. Hamedi, T. Kirova, and E. Paspalakis, Phys. Rev. A **105**, 043709 (2022).
[27] L. Wang, F. Zhou, P. Hu, Y. Niu, and S. Gong, J. Phys. B: At. Mol. Opt. Phys. **47**, 225501 (2014).
[28] F. Evers and A. D. Mirlin, Phys. Rev. Lett. **84**, 3690 (2000).